Effect of Electroplating Additives on Copper Protrusion of Metallized Through-Glass Vias (TGVs)

Qichang An*, Chuncheng Che*, Yue Li*, Hongjie Zhao*, Xiaodong Li*, Yingying Zhao*, Yuelei Xiao*, Xuecheng Hou*

**** Beijing BOE Sensor Technology Company, Ltd., Beijing, China***

Abstract

Glass demonstrates exceptional high-frequency performance due to its superior dielectric properties. This work proposes impurities from additives cause vacancies, which, under thermal stress due to CTE mismatch between Cu and glass, aggregate and lead to Cu protrusion of TGV-Cu. Reducing impurity can minimize protrusion, enhancing the reliability of TGV-Cu structures.

Author Keywords

TGV-Cu; protrusion; impurity; void

1. Introduction

Glass exhibits excellent high-frequency performance due to its superior dielectric properties, making it ideal for minimizing insertion losses in high-frequency devices.[1-4] Additionally, glass offers a tunable coefficient of thermal expansion (CTE) and other desirable physical characteristics, allowing it to be engineered to align with the material properties of surrounding dissimilar materials. Glass-based devices can also be manufactured on large panels, enabling cost-effective high-volume production. To achieve miniaturization and enhance electrical performance, 2.5D and 3D chip architectures employing vertical interconnect technology have been widely adopted in high-end products.[5,6] Through-glass vias (TGV) technology facilitates the creation of vertical interconnects within a glass substrate, where the vias are filled with conductive material to achieve electrical connectivity. Copper is the most commonly used material for filling TGVs due to its excellent electrical properties.

However, metallized TGVs present significant thermo-mechanical challenges during high-temperature processes, primarily due to the substantial CTE mismatch between Cu (16.7 ppm/°C) and glass (3.3 ppm/°C for BOROFLOAT®33), which differs by nearly six times. The copper, being enclosed by the glass substrate, undergoes pronounced thermal expansion at elevated temperatures, often resulting in macroscopic manifestations of Cu protrusion that can lead to interfacial failure.[7,8]

In this study, a novel mechanism for Cu protrusion in TGV-Cu is proposed. The influence of electroplating impurities, derived from organic additives in the plating solution, on Cu protrusion is investigated through the observation and measurement of TGV-Cu protrusion and microstructures following heat treatment.

2. Experiments

The geometrical structure of TGV-Cu is illustrated in **Figure 1**. The glass wafers used in this study are 8 inches in size and have a thickness of 0.645 mm. The blind Cu vias are periodically arranged with a diameter of 55 µm, a depth of 270 µm, an 87° taper angle, and a pitch distance of 110 µm.

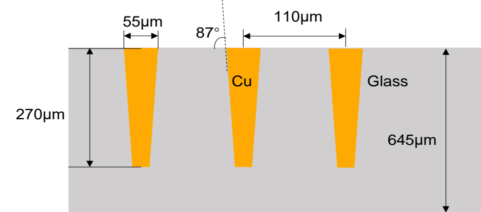

Figure 1. Geometrical model of TGV-Cu structure.

The TGV wafers utilized in this study are fabricated through a series of processes, as shown in **Figure 2(a)**. The fabrication begins with laser-induced deep etching (LIDE) of glass wafers to form the vias. Next, an adhesion layer of titanium (Ti) and a copper (Cu) seed layer are deposited via physical vapor deposition (PVD). Based on this seed layer, the vias are subsequently filled with copper through an electroplating process. The electroplating setup, shown in **Figure 2(b)**, consists of a Ti/Cu-deposited TGV substrate as the cathode, a Cu plate as the anode, and an electrolyte containing high-purity $CuSO_4$ and H_2SO_4. Additionally, organic additives, including accelerators, inhibitors, and levelers, are introduced to the plating solution to optimize the deposition. These additives promote bottom-up filling of the TGV, and inhibit deposition near via opening and wafer surface, to ensure complete filling without voids. The concentrations and types of additives are carefully optimized to control impurity levels within the TGV-Cu. In this study, two different TGV-Cu samples are fabricated using distinct electroplating additives. The two types of wafers are designated as TGV_1 (using Additive 1) and TGV_2 (using Additive 2).

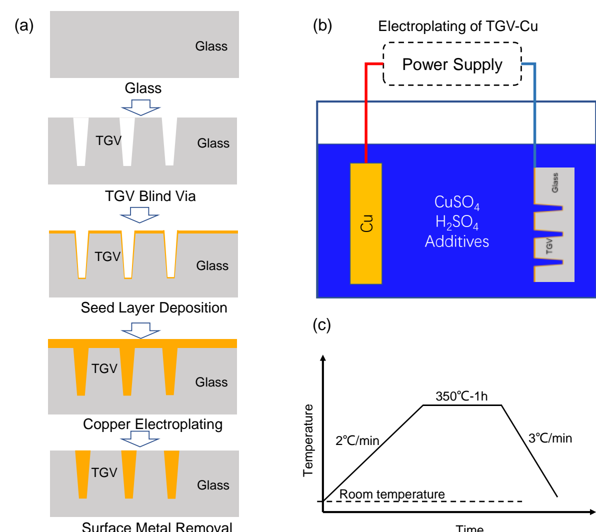

Figure 2. (a) Process flow of TGV wafer. (b) Electroplating setup for TGV-Cu. (c) Annealing profile.

ISSN 0097-996X/25/5602-1109-$1.00 © 2025

Following electroplating, residual Cu on the wafer surface is removed through chemical-mechanical polishing (CMP). With no overlaying layer on the TGVs, the TGV-Cu is free to expand or contract, enabling direct observation of Cu protrusion. A peak annealing temperature of 350 °C is chosen to investigate the Cu protrusion phenomenon. As shown in **Figure 2(c)**, TGV_1 and TGV_2 wafers are heated from room temperature to 350 °C at a rate of 2 °C/min, then held at 350 °C for 1 hour, followed by cooling to room temperature at a rate of 3 °C/min. Nitrogen gas is used to prevent oxidation during the annealing process.

The surface morphology of the TGV vias is observed using an optical microscope (OM) both before and after heat treatment. OM observations are employed to identify local Cu protrusions generated after annealing. The heights of global and local Cu protrusions are subsequently measured using a confocal laser scanning microscope (CLSM). Additionally, focused ion beam (FIB) milling is performed on the top areas of selected TGVs, followed by cross-sectional characterization using a scanning electron microscope (SEM).

3. Results

The surface morphology of TGV_1-Cu and TGV_2-Cu is characterized using an optical microscope (OM) before and after heat treatment. After heat treatment, noticeable global Cu protrusions are observed in TGV_1-Cu wafers, while local Cu protrusions are detected in TGV_2 wafers. **Figure 3(a)** shows the top view of Cu vias after electroplating, and **Figure 3(b)** presents the top view of Cu vias after CMP. Following heat treatment at 350 °C, **Figure 3(c)** illustrates the top view of TGV_1 wafers with evident global protrusions of TGV_1-Cu, while **Figure 3(d)** shows the top view of TGV_2 wafers, revealing local protrusions of TGV_2-Cu.

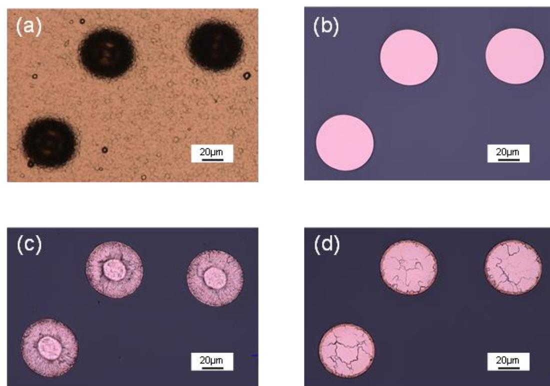

Figure 3. (a) Optical microscopic image of the TGV-Cu after electroplating, (b) Optical microscopic image of the TGV-Cu after CMP (before heat treatment), (c) Optical microscopic image of the TGV_1-Cu after 350 °C heat treatment, (d) Optical microscopic image of the TGV_2-Cu after 350 °C heat treatment.

To quantify and compare the protrusion heights of TGV1-Cu and TGV2-Cu, measurements are taken using confocal laser scanning microscopy (CLSM). Figure 4(a) and 4(b) show 2D laser images of TGV1-Cu and TGV2-Cu after heat treatment, respectively. For 3D morphology profiling, the laser is set to vertical scanning mode, and the height profiles are extracted along the centerline of the TGV-Cu columns, as shown in Figure 4(c) and 4(d). The results indicated significant Cu protrusions in both samples relative to the surrounding glass substrate. The average global Cu protrusion height in TGV1-Cu is 6.826 μm, while the average local Cu protrusion height in TGV2-Cu is 0.875 μm. A comparison between the two samples revealed that the protrusion heights of TGV1-Cu are substantially higher than those of TGV2-Cu, suggesting distinct mechanisms for global and local protrusions. The greater protrusion heights imply a higher risk of inducing structural distortion and fracture around the TGV, highlighting the importance of investigating the underlying mechanism of Cu protrusion.

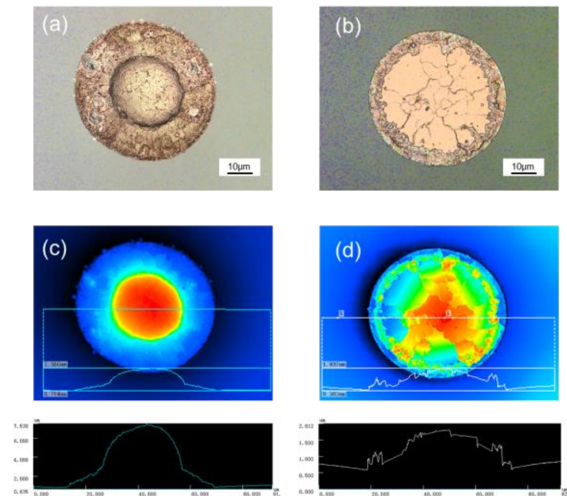

Figure 4. CLSM laser images of (a) TGV_1-Cu and (b) TGV_2-Cu. CLSM image of 3D morphology and height profiles of (c) TGV_1-Cu and (d) TGV_2-Cu after 350 °C heat treatment.

The surface and cross-sectional morphologies of TGV1-Cu and TGV2-Cu vias are further analyzed using FIB-SEM, as shown in Figure 5. After the 350 °C heat treatment, Figure 5(a) and (b) confirm the presence of pronounced global Cu protrusions in TGV1-Cu and local Cu protrusions in TGV2-Cu, respectively. The Cu surfaces after CMP appeared flat. The protrusion height in TGV1-Cu increased towards the center of the vias, reaching nearly 7 μm, consistent with CLSM measurements. In contrast, the protrusion height in TGV2-Cu is smaller. Figure 5(e) reveals that the global protrusions in TGV1-Cu consisted of numerous Cu grains and voids, with the void density increasing towards the center of the vias. Figure 5(f) shows that the local protrusions in TGV2-Cu comprised several Cu grains, with the protrusion boundaries aligning with the grain boundaries at the top region of the TGV-Cu, as indicated by red circles in Figures 5(b) and 5(f). Notably, no voids are observed in TGV2-Cu.

Energy dispersive X-ray spectroscopy (EDX) analyses, shown in **Figure 6**, demonstrated a significant contrast in impurity concentrations (C, Cl, S, O, N) between TGV_1-Cu and TGV_2-Cu. TGV_1-Cu exhibited much higher impurity levels, likely due to the differences in electroplating additives (Additive 1 and Additive 2).

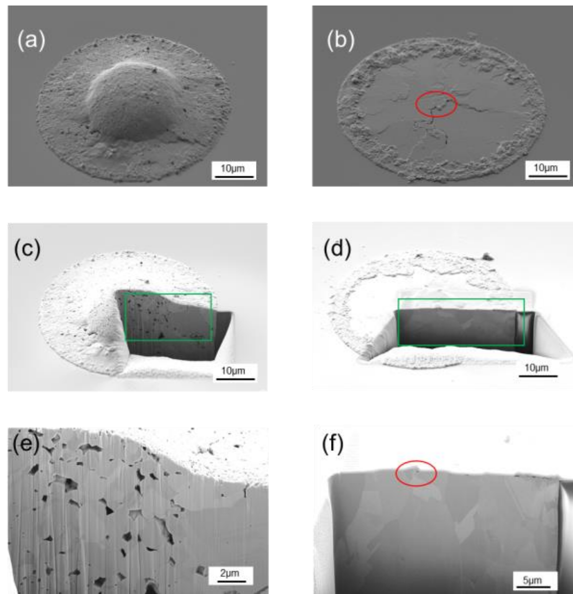

Figure 5. Surface SEM results of TGV-Cu in (a) TGV_1-Cu and (b) TGV_2-Cu after 350 °C heat treatment before FIB milling. SEM images of TGV-Cu in (c) TGV_1-Cu and (d) TGV_2-Cu after FIB milling. Cross-section SEM images of TGV-Cu in (e) TGV_1-Cu and (f) TGV_2-Cu.

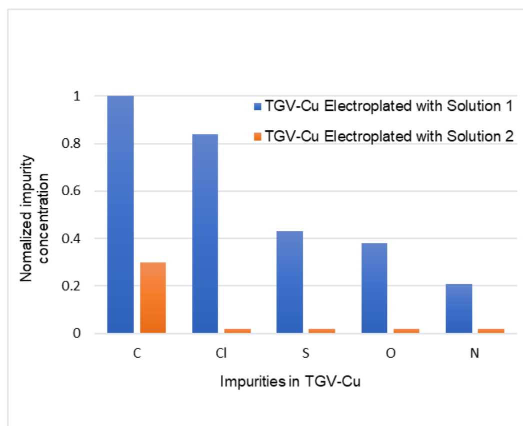

Figure 6. EDX analyses for normalized impurities concentration of TGV_1-Cu and TGV_2-Cu.

4. Discussion

To further explore the mechanisms underlying Cu protrusion, two types of Cu protrusions are analyzed from the perspectives of impurity incorporation, induced thermal stress, and vacancy aggregation. During the electroplating of TGV_1-Cu, impurities originating from the organic substance in the plating solution (Additive 1) co-deposited with Cu.[9] This impurity incorporation increases atomic disarrangement, leading to the formation of numerous vacancies within TGV_1-Cu that aggregates along Cu grain boundaries, as illustrated in **Figure 7(a)**. In contrast, substituting the additive leads to minimal impurity incorporation in TGV_2-Cu, resulting in fewer vacancies, as shown in **Figure 7(b)**.

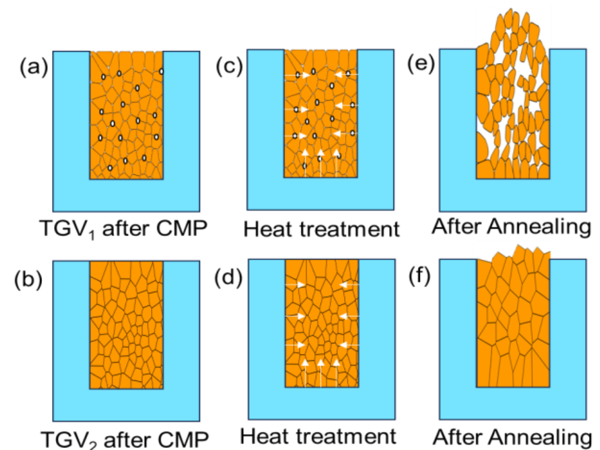

Figure 7. Schematic of microstructures in (a) TGV_1-Cu and (b) TGV_2-Cu at the initial state after CMP. Schematic of microstructures during heat treatment in (c) TGV_1-Cu and (d) TGV_2-Cu. Schematic of microstructures after annealing at 350 °C in (e) TGV_1-Cu and (f) TGV_2-Cu. White arrows indicate the direction of thermal stress exerted on TGV-Cu by the surrounding glass substrate.

The initial TGV-Cu structures nearly possess a stress-free state after CMP at room temperature. During the heat treatment at 350 ℃, TGV-Cu and glass substrate tend to expand due to the increasement of atomic thermal vibration at high temperature. Due to the large CTE mismatch between Cu and glass, the free expansion of TGV-Cu is locked by the surrounding glass. This trend can lead to an axial and radial compressive stress exerted on TGV-Cu, as illustrated by the white arrows in Figure 7(c) and 7(d). The vacancies distributed along the Cu grains boundaries can be driven to migrate from edge to center by the axial and radial thermal stress, and void formation in center is induced by the aggregation of vacancies. This can explain the phenomenon that global protrusion and voids in center of TGV1-Cu, as shown in Figure 7(e) and Figure 5(e). In addition, as the temperature of heat treatment is 350 ℃, thermal stress is large enough to induce plastic deformation of Cu, and local plastic deformation occurs in the TGV-Cu, as shown in Figure 7(f) and Figure 5(f). The difference of additives in plating solution between TGV1-Cu and TGV2-Cu is the reason for different Cu protrusion behaviors in the TGV-Cu.

To maintain the mechanical and electrical interconnections between TGV-Cu and the redistribution layer (RDL), it is crucial to prevent Cu protrusion after heat treatment. Based on the findings, optimizing the plating solution additives is essential to minimize impurity and vacancy concentrations in TGV-Cu. A TGV_2-Cu structure integrated with RDL is fabricated, and after heat treatment at 350 °C for 1 hour, cross-sectional SEM characterization is performed, as shown in **Figure 8**. The results demonstrates a strong bond between TGV_2-Cu and the RDL, indicating that optimizing the additives effectively can mitigate Cu protrusion.

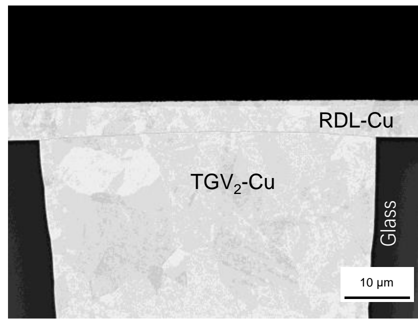

Figure 8. Cross-section SEM results of TGV_2-Cu structure with RDL after 350 °C heat treatment.

5. Conclusion

This study demonstrates, for the first time, the connection between Cu protrusion in TGV-Cu and the choice of electroplating additives. By utilizing two different additives, the varying behaviors of Cu protrusion are analyzed. Impurities introduced by certain additives lead to the formation of vacancies within TGV-Cu. Under thermal stress induced by the CTE mismatch between Cu and the glass substrate, these vacancies migrate and aggregate at the center, resulting in significant Cu protrusion after heat treatment. To mitigate the adverse effects of large protrusions, the selection and optimization of electroplating additives are crucial. This work presents a new mechanism for Cu protrusion in Cu-filled TGV structures, contributing valuable insights to improve the thermomechanical and electrical reliability of TGV technology.

6. References

1. Kim, Y., Cho, J., Kim, K., Sundaram, V., Tummala, R., & Kim, J. (2015, May). Signal and power integrity analysis in 2.5 D integrated circuits (ICs) with glass, silicon and organic interposer. In *2015 IEEE 65th Electronic Components and Technology Conference (ECTC)* (pp. 738-743). IEEE.
2. Hwangbo, S., Yoon, Y. K., & Shorey, A. (2016, June). Glass interposer integrated dual-band millimeter wave TGV antenna for inter-/intra chip and board communications. In *2016 IEEE International Symposium on Antennas and Propagation (APSURSI)* (pp. 1639-1640). IEEE.
3. Lee, T. C., Chang, Y. S., Hsu, C. M., Hsieh, S. C., Lee, P. N., Hsieh, Y. C., ... & Zhang, L. (2017, May). Glass Based 3D-IPD Integrated RF ASIC in WLCSP. In *2017 IEEE 67th Electronic Components and Technology Conference (ECTC)* (pp. 631-636). IEEE.
4. An, Q., Xiao, Y., Li, Y., Xu, S., Zhao, Y., Hou, X., ... & Che, C. (2024, June). P-136: Process Optimization for Fabrication of 3D Through Glass Via (TGV) Inductor. In *SID Symposium Digest of Technical Papers* (Vol. 55, No. 1, pp. 1914-1917).
5. Chien, C. H., Lee, C. K., Yu, H., Liu, C. C., Chen, P. S., Chien, H. C., ... & Lu, Y. J. (2013, January). Performance and process comparison between glass and Si interposer for 3D-IC integration. In *International Symposium on Microelectronics* (Vol. 2013, No. 1, pp. 000618-000624). International Microelectronics Assembly and Packaging Society.
6. Wang, H., Wang, J., Xu, J., Pham, V., Pan, K., Park, S., ... & Refai-Ahmed, G. (2019, May). Product level design optimization for 2.5 D package pad cratering reliability during drop impact. In *2019 IEEE 69th Electronic Components and Technology Conference (ECTC)* (pp. 2343-2348). IEEE.
7. An, Q., Xiao, Y., Wei, Q., Wu, Y., Li, H., & Li, Y. (2023, June). 75-2: Failure Mechanisms and Optimum Methods for Through Glass Via. In *SID Symposium Digest of Technical Papers* (Vol. 54, No. 1, pp. 1060-1063).
8. Wang, H., Lai, C., Ma, B., Jian, X., Chen, S., Chen, H., ... & Yang, X. (2024, August). Failure Mechanisms Investigation of Through Glass via (TGV) Under Thermal Annealing and Shock. In *2024 25th International Conference on Electronic Packaging Technology (ICEPT)* (pp. 1-6). IEEE.
9. Chiang, P. C., Shen, Y. A., & Chen, C. M. (2021). Effects of impurities on void formation at the interface between Sn-3.0 Ag-0.5 Cu and Cu electroplated films. *Journal of Materials Science: Materials in Electronics*, 32, 11944-11951.